

# Periodic Solutions of the Serre Equations

John D. Carter  
carterj1@seattleu.edu  
phone: (206) 296-5956  
fax: (206) 296-5932  
Mathematics Department  
Seattle University  
901 12<sup>th</sup> Avenue  
Seattle, WA 98122

Rodrigo Cienfuegos  
racienfu@ing.puc.cl  
phone: (56 2) 354-4227  
fax: (56 2) 354-5876  
Depto. Ingeniería Hidráulica y Ambiental  
Pontificia Universidad Católica de Chile  
Av. Vicuña Mackenna 4860 - Macul  
Santiago de Chile

## 1 Abstract

The Serre equations are a pair of strongly nonlinear, weakly dispersive, Boussinesq-type partial differential equations. They model the evolution of the surface elevation and the depth-averaged horizontal velocity of an inviscid, irrotational, incompressible fluid on a horizontal bottom. We present a three-parameter family of periodic solutions of the Serre equations and examine their linear stability. We establish that waves with sufficiently small amplitude/steepness are stable while waves with sufficiently large amplitude/steepness are unstable.

## 2 Introduction

The evolution of gravity waves on the surface of an inviscid, incompressible fluid can be modeled by the Euler equations or by means of the potential flow theory under the additional constraint of irrotationality. For many applications in the nearshore zone it is customary to derive approximate versions of the complete Euler or potential flow systems by using a small-parameter perturbation procedure as done for example by Madsen & Schäffer [12]. Generally, the derivation of these simplified models requires the introduction of the following standard dimensionless parameters

$$\epsilon = \frac{A_0}{H_0} \quad \text{and} \quad \delta = \frac{H_0}{L_0}. \quad (1)$$

Here  $A_0$ ,  $H_0$  and  $L_0$  are positive constants representing a typical wave amplitude, the depth of the undisturbed fluid, and a typical wavelength in the horizontal dimension respectively. The parameter  $\epsilon$  measures nonlinearity and  $\delta$  measures dispersion. In addition, the steepness parameter,  $\Lambda$ , is defined as follows

$$\Lambda = 2\frac{A_0}{L_0} = 2\epsilon\delta. \quad (2)$$

Figure 1 contains a plot of the physical system and graphically defines all parameters.

Recently, much progress has been made in providing a solid theoretical background for Boussinesq-type wave equations from both mathematical and engineering standpoints. These equations are approximations to the full Euler or potential flow systems and can be derived following the classic work of Boussinesq [3], Rayleigh [13], or by using a small-parameter expansion. Bona, Chen & Saut [2] provide a thorough review of many Boussinesq-type models for small-amplitude, weakly dispersive waves.

When no assumption is made on the order of magnitude of  $\epsilon$ , large-amplitude waves propagating in shallow water can be described. The first strongly nonlinear, weakly dispersive set of Boussinesq-type equations was derived by Serre [15, 16]. Several years later, Su & Gardner [17] and Green & Naghdi [9] re-derived the Serre equations using different methods. A formal derivation using series expansion on small

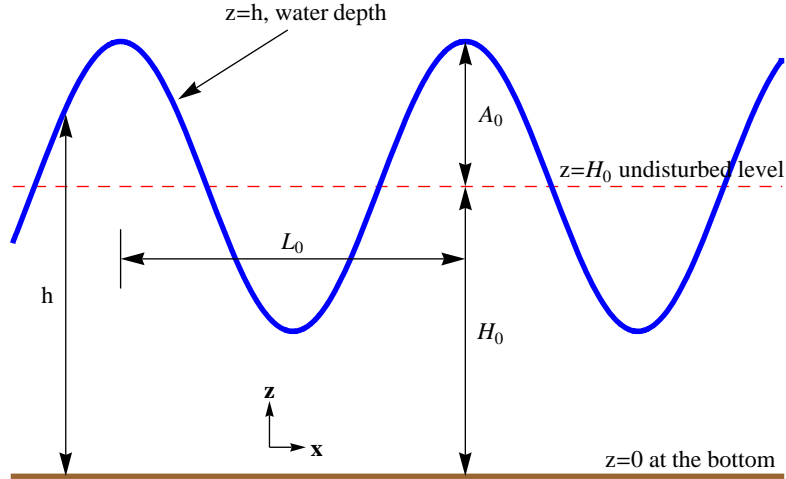


Figure 1: The physical system and parameters under consideration.

perturbation parameters is presented by Barthélemy [1] for horizontal bottoms and by Cienfuegos *et al.* [5] for non-horizontal bottoms. The Serre equations are obtained by depth-averaging the full Euler system and truncating the resulting set of equations at  $\mathcal{O}(\delta^4)$  without making any assumptions on the order of  $\epsilon$ . This “full nonlinearity” makes the Serre equations ideal for studying large-amplitude or nearly breaking waves in the nearshore zone.

The accuracy of the Serre equations in describing strongly nonlinear shallow water waves has been confirmed by comparisons between numerical simulations and physical experiments including solitary waves propagating over a step [14], solitary waves shoaling over different slopes [1, 6], and regular wave shoaling and breaking over uniform beach slopes where extra terms had to be incorporated to account for energy dissipation [7]. Guizien & Barthélemy [10] generated solitary waves in a flume with minimal trailing waves by using the solitary wave solution to the Serre equations. Finally, the theoretical analysis of Lannes & Bonneton [11] shows that the Serre equations constitute a relevant system to model highly nonlinear waves propagating in shallow waters.

In this paper, we investigate additional properties of the Serre equations related to the existence of closed-form periodic solutions and their stability. Section 3 contains some mathematical properties of the Serre equations including a three-parameter family of periodic solutions. Section 4 contains our main result: waves with sufficiently small amplitude/steepness are stable while waves with sufficiently large amplitude/steepness are unstable.

### 3 The Serre Equations

The dimensional Serre equations for water on a horizontal bottom are [1],

$$h_t + (hu)_x = 0, \quad (3a)$$

$$u_t + uu_x + gh_x - \frac{1}{3h} \left( h^3 (u_{xt} + uu_{xx} - (u_x)^2) \right)_x = 0, \quad (3b)$$

where  $u = u(x, t)$  is the depth-averaged horizontal velocity of the fluid,  $h = h(x, t)$  is the water depth, and  $g$  is the acceleration due to gravity. We focus this pair of equations with periodic boundary conditions, though we make a few comments regarding the solitary-wave limit.

The Serre equations admit the following conservation laws

$$\partial_t(h) + \partial_x(hu) = 0, \quad (4a)$$

$$\partial_t(hu) + \partial_x \left( \frac{1}{2}gh^2 + hu^2 - \frac{1}{3}h^3u_{xt} + \frac{1}{3}h^3u_x^2 - \frac{1}{3}h^3uu_{xx} \right) = 0, \quad (4b)$$

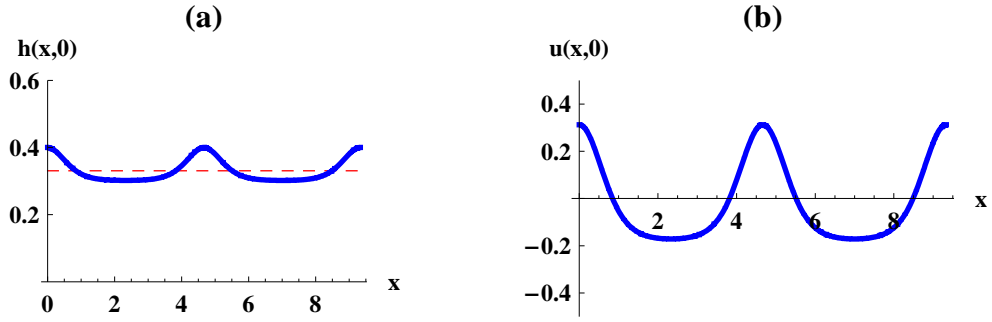


Figure 2: Plots of the water depth,  $h$ , and depth-averaged horizontal velocity,  $u$ , corresponding to the solution given in equation (6) with  $k = 0.99$ ,  $a_0 = 0.3$  and  $a_1 = 0.1$  at  $t = 0$ . The dashed line in (a) represents the mean water depth.

$$\partial_t \left( \frac{1}{2} h (gh + u^2 + \frac{1}{3} h^2 u_x^2) \right) + \partial_x \left( hu (gh + \frac{1}{2} u^2 + \frac{1}{2} h^2 u_x^2 - \frac{1}{3} h^2 (u_{xt} + uu_{xx})) \right) = 0. \quad (4c)$$

Equation (4a) corresponds to conservation of mass, (4b) corresponds to conservation of momentum, and (4c) corresponds to conservation of energy.

The Serre equations are invariant under the following transformation

$$h(x, t) = \hat{h}(x - st, t), \quad (5a)$$

$$u(x, t) = s + \hat{u}(x - st, t), \quad (5b)$$

$$\hat{x} = x - st, \quad (5c)$$

where  $s$  is a free parameter. This transformation physically represents adding a constant horizontal velocity  $s$  to the entire system.

The Serre equations admit the following family of solutions

$$h(x, t) = a_0 + a_1 \text{dn}^2(\kappa(x - ct), k), \quad (6a)$$

$$u(x, t) = c \left( 1 - \frac{h_0}{h(x, t)} \right), \quad (6b)$$

$$\kappa = \frac{\sqrt{3a_1}}{2\sqrt{a_0(a_0 + a_1)(a_0 + (1 - k^2)a_1)}}, \quad (6c)$$

$$c = \frac{\sqrt{ga_0(a_0 + a_1)(a_0 + (1 - k^2)a_1)}}{h_0}, \quad (6d)$$

where  $k \in [0, 1]$ ,  $a_0 > 0$  and  $a_1 > 0$  are real parameters. Here  $\text{dn}(\cdot, k)$  is a Jacobi elliptic function with elliptic modulus  $k$  [4]. The mean water depth,  $h_0$ , is defined by

$$h_0 = \frac{\kappa}{2K(k)} \int_0^{2K(k)/\kappa} h(x, t) dx = a_0 + a_1 \frac{E(k)}{K(k)}, \quad (7)$$

where  $K(k)$  and  $E(k)$  are the complete elliptic integrals of the first and second kinds respectively. Figure 2 contains representative plots of  $h$  and  $u$ .

If  $k \in (0, 1)$ , the solutions given in equation (6) are spatially periodic with period  $2K(k)/\kappa$ . As  $k \rightarrow 0^+$ , these solutions limit to

$$h(x, t) = a_0 + a_1, \quad (8a)$$

$$u(x, t) = 0. \quad (8b)$$

In other words, as  $k \rightarrow 0^+$ , the solutions given in equation (6) limit to the trivial solution of a zero-velocity fluid with a horizontal surface at  $a_0 + a_1$ .

As  $k \rightarrow 1^-$ , the family of periodic solutions limits to the following two-parameter family of solitary-wave solutions

$$h(x, t) = a_0 + a_1 \operatorname{sech}^2(\kappa(x - ct)), \quad (9a)$$

$$u(x, t) = c \left( 1 - \frac{a_0}{h(x, t)} \right), \quad (9b)$$

$$\kappa = \frac{\sqrt{3a_1}}{2a_0\sqrt{a_0 + a_1}}, \quad (9c)$$

$$c = \sqrt{g(a_0 + a_1)}. \quad (9d)$$

This solution is known as the Rayleigh solitary wave solution.

## 4 Linear Stability

In order to study the linear stability of the solutions given in equation (6), we enter a coordinate frame moving with the velocity of the waves via the following transformation

$$\chi = x - ct, \quad (10a)$$

$$\tau = t, \quad (10b)$$

where  $c$  is defined in equation (6d). After this change of variables, the Serre equations are

$$h_\tau - ch_\chi + (hu)_\chi = 0, \quad (11a)$$

$$u_\tau - cu_\chi + uu_\chi + gh_\chi - \frac{1}{3h} \left( h^3 (u_{\chi\tau} - cu_{\chi\chi} + uu_{\chi\chi} - (u_\chi)^2) \right)_\chi = 0, \quad (11b)$$

and the solutions given in equation (6) simplify to the following time-independent solutions

$$h = \eta_0(\chi) = a_0 + a_1 \operatorname{dn}^2(\kappa\chi, k), \quad (12a)$$

$$u = u_0(\chi) = c \left( 1 - \frac{h_0}{h(\chi)} \right), \quad (12b)$$

where  $\kappa$ ,  $c$ , and  $h_0$  are defined in equations (6c), (6d) and (7) respectively.

We consider perturbed solutions of the form

$$h_{\text{pert}}(\chi, \tau) = \eta_0(\chi) + \mu\eta_1(\chi, \tau) + \mathcal{O}(\mu^2), \quad (13a)$$

$$u_{\text{pert}}(\chi, \tau) = u_0(\chi) + \mu u_1(\chi, \tau) + \mathcal{O}(\mu^2), \quad (13b)$$

where  $\eta_1$  and  $u_1$  are real-valued functions and  $\mu$  is a small real parameter. Substituting equation (13) into equation (11) and linearizing leads to a pair of coupled, linear partial differential equations that are constant coefficient in  $\tau$ . Without loss of generality, assume

$$\eta_1(\chi, \tau) = H(\chi)e^{\Omega\tau} + c.c., \quad (14a)$$

$$u_1(\chi, \tau) = U(\chi)e^{\Omega\tau} + c.c., \quad (14b)$$

where  $H(\chi)$  and  $U(\chi)$  are complex-valued functions,  $\Omega$  is a complex constant, and  $c.c.$  denotes complex conjugate. If  $\Omega$  has a positive real part, then the perturbations  $\eta_1$  and  $u_1$  grow exponentially in  $\tau$  and the solution is said to be linearly unstable. Further, if the real part of  $\Omega$ ,  $\Re(\Omega)$ , is positive, we define it to be the growth rate of the perturbation.

Substituting (14) into the linearized system of PDEs gives

$$\mathcal{L} \begin{pmatrix} H \\ U \end{pmatrix} = \Omega \mathcal{M} \begin{pmatrix} H \\ U \end{pmatrix}, \quad (15)$$

Case I			
$a_1$	$\delta$	$\epsilon$	$\Lambda$
0.05	0.0922	0.0420	0.0077
0.1	0.1302	0.0762	0.0198
0.2	0.1841	0.1284	0.0473
0.3	0.2258	0.1664	0.0751

Table 1: The values of  $a_1$ ,  $\delta$ ,  $\epsilon$  and  $\Lambda$  for the Case I numerical simulations.

where  $\mathcal{L}$  and  $\mathcal{M}$  are the linear differential operators defined by

$$\mathcal{L} = \begin{pmatrix} -u'_0 + (c - u_0)\partial_\chi & -\eta'_0 - \eta_0\partial_\chi \\ \mathcal{L}_{21} & \mathcal{L}_{22} \end{pmatrix}, \quad (16a)$$

$$\mathcal{M} = \begin{pmatrix} 1 & 0 \\ 0 & 1 - \eta_0\eta'_0\partial_\chi - \frac{1}{3}\eta_0^2\partial_{\chi\chi} \end{pmatrix}, \quad (16b)$$

where prime represents derivative with respect to  $\chi$  and

$$\mathcal{L}_{21} = -\eta'_0(u'_0)^2 - c\eta'_0u''_0 - \frac{2}{3}c\eta_0u'''_0 + \eta'_0u_0u''_0 - \frac{2}{3}\eta_0u'_0u''_0 + \frac{2}{3}\eta_0u_0u'''_0 + (\eta_0u_0u''_0 - g - \eta_0(u'_0)^2 - c\eta_0u''_0)\partial_\chi, \quad (17a)$$

$$\mathcal{L}_{22} = -u'_0 + \eta_0\eta'_0u''_0 + \frac{1}{3}\eta_0^2u'''_0 + (c - u_0 - 2\eta_0\eta'_0u'_0 - \frac{1}{3}\eta_0^2u''_0)\partial_\chi + (\eta_0\eta'_0u_0 - c\eta_0\eta'_0 - \frac{1}{3}\eta_0^2u'_0)\partial_{\chi\chi} + (\frac{1}{3}\eta_0^2u_0 - \frac{1}{3}c\eta_0^2)\partial_{\chi\chi\chi}. \quad (17b)$$

The system given in equation (15), subject to periodic boundary conditions, is a differential eigenvalue problem. The eigenvalues,  $\Omega$ s, determine how the perturbations evolve in  $\tau$ . The corresponding eigenfunctions,  $H$  and  $U$ , determine the  $\chi$  structure of the perturbations.

In order to find approximations to the eigenvalues and eigenfunctions corresponding to the solutions given in equation (12), we employ the Fourier-Floquet-Hill (FFH) method of Deconinck & Kutz [8]. This numerical method is spectrally accurate for differential eigenvalue problems with periodic coefficients (such as the one under consideration here) and allows the computation of eigenfunctions of the form

$$\begin{pmatrix} H \\ U \end{pmatrix} = e^{i\rho\chi} \begin{pmatrix} H^P \\ U^P \end{pmatrix}, \quad (18)$$

where  $H^P$  and  $U^P$  are periodic in  $\chi$  with period  $2K/\kappa$  and  $\rho \in [-\pi\kappa/(4K), \pi\kappa/(4K)]$ . Therefore, if  $\rho = 0$ , then the perturbation has the same period as the unperturbed solution.

In the remainder of this section, we present results from numerical simulations. Our plots focus on regions where  $\Re(\Omega) > 0$  because these are the values that establish instability. Further, symmetries of the system establish that the second, third, and fourth quadrants of the complex- $\Omega$  plane are reflections of the first quadrant.

#### 4.1 Case I: Fixed $a_0$ and $k$

Figure 3 contains plots of spectra obtained using the FFH method with 75 positive Fourier modes (a measure of spectral resolution) and 1500 different  $\rho$  values (a measure of the number of different quasi-periods examined). For this series of numerical simulations,  $a_0 = 0.3$  and  $k = 0.75$  were fixed while  $a_1$  was varied. Changing the value of  $a_1$  changes the amplitude and the period of the solution. As  $a_1$  increases,  $\delta$ ,  $\epsilon$  and  $\Lambda$  all increase. The values of the nonlinearity, dispersion and steepness parameters for these simulations are included in Table 1.

##### Observations:

- If  $a_1$  is small enough, there are no  $\Omega$ s with positive real part and therefore the solution is linearly stable. This establishes that (in this parameter regime) waves with sufficiently small amplitude are stable.

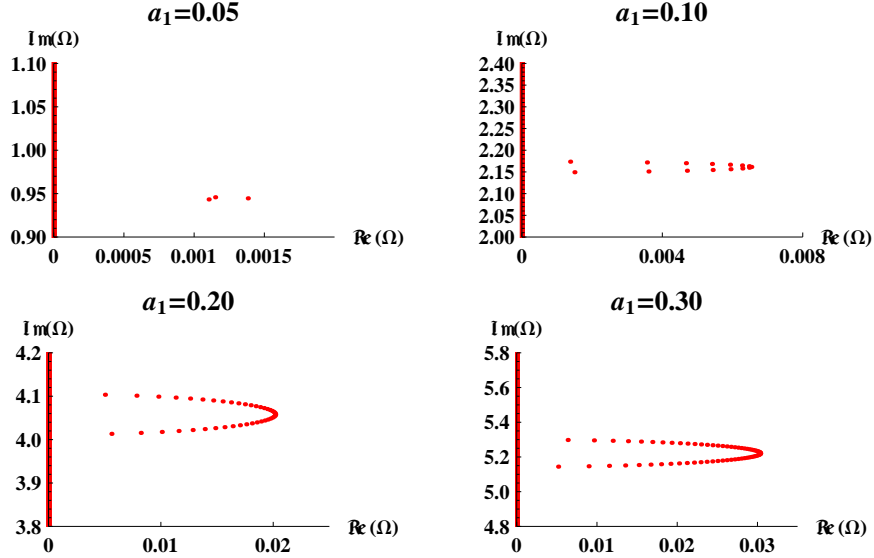


Figure 3: Results from Case I numerical simulations. A discrete representation of the spectra of (15) corresponding to  $a_0 = 0.3$ ,  $k = 0.75$  and four different values of  $a_1$ .

- If  $a_1$  is large enough, then there are  $\Omega$ s with positive real parts and therefore the solution is linearly unstable. This establishes that waves with sufficiently large amplitude are unstable.
- The cutoff between stability and instability occurs at  $a_1 \approx 0.023$ .
- The maximum growth rate increases as  $a_1$  increases.
- All instabilities are oscillatory instabilities. That is, every  $\Omega$  that has a positive real part has a nonzero imaginary part.
- The rate of instability oscillation,  $\Im(\Omega)$ , (the imaginary part of  $\Omega$ ) increases as  $a_1$  increases.
- For these parameter values, there is only one band of instabilities for each value of  $a_1$ . In the first quadrant, each of these bands is a half oval.
- Generally, the instability with maximal growth rate corresponds to a perturbation with nonzero  $\rho$ . This means that the period of the most unstable mode is longer than that of the unperturbed solution.

## 4.2 Case II: Fixed $a_0$ and $a_1$

Figure 4 contains plots of spectra obtained using the FFH method with 75 positive Fourier modes and 1500  $\rho$  values. For this series of numerical simulations,  $a_0 = 0.3$  and  $a_1 = 0.1$  were fixed while  $k$  was varied. Changing the parameter  $k$  changes the amplitude, period and steepness of the wave. As  $k$  increases,  $\epsilon$  increases,  $\delta$  decreases, and  $\Lambda$  increases up to  $k \approx 0.925$  and then decreases. The values of  $\epsilon$ ,  $\delta$  and  $\Lambda$  corresponding to the Case II numerical simulations are included in Table 2.

### Observations:

- If  $k$  is small enough, there is no instability. If  $k$  is large enough, there is instability. This establishes that waves with sufficiently small steepness/amplitude are stable and that waves with sufficiently large steepness/amplitude are unstable.
- The cutoff between stability and instability occurs at  $k \approx 0.30$ .

Case II			
$k$	$\delta$	$\epsilon$	$\Lambda$
0.5	0.1482	0.0323	0.0096
0.9	0.1078	0.1153	0.0249
0.99	0.0708	0.1482	0.0210
0.999	0.0517	0.1548	0.0160

Table 2: The values of  $k$ ,  $\delta$ ,  $\epsilon$  and  $\Lambda$  for the Case II numerical simulations.

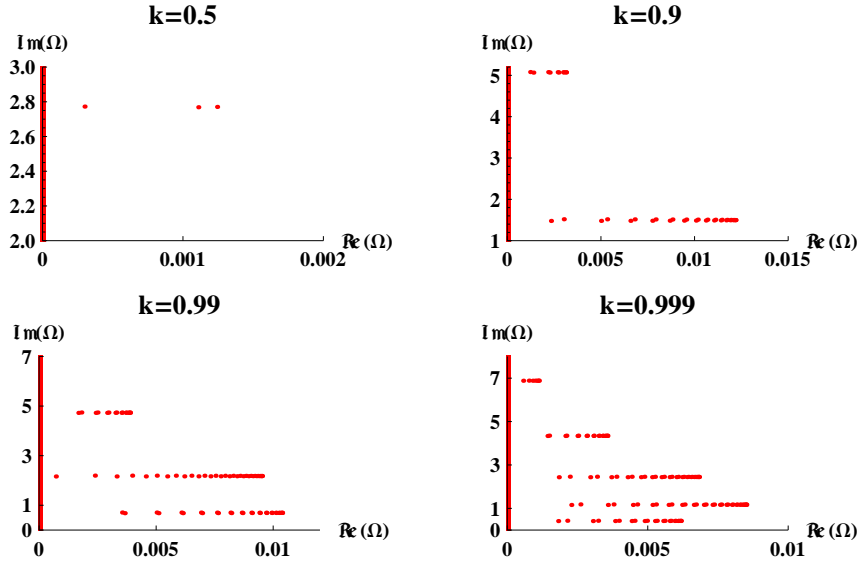


Figure 4: Results from Case II numerical simulations. A discrete representation of the spectra of (15) corresponding to  $a_0 = 0.3$ ,  $a_1 = 0.1$  and four different values of  $k$ .

- Each of the bands in the first quadrant is a compressed half oval. As  $k$  increases, the number of bands of instability increases.
- All instabilities are oscillatory instabilities.
- As  $k$  increases away from zero, the maximum growth rate increases until  $k \approx 0.947$ . Above this value, the maximum growth rate decreases. At  $k = 0.947$ , the maximum growth rate is 0.0132.
- Generally, the instability with maximal growth rate is a  $\rho \neq 0$  perturbation.

### 4.3 Case III: Fixed $a_0$ and wave amplitude

Figure 5 contains plots of spectra obtained using the FFH method with 75 positive Fourier modes and 1500  $\rho$  values. For this series of numerical simulations,  $a_0$  and the wave height,  $a_1 k^2$ , were fixed at 0.3 and 0.1 respectively. The parameters  $k$  and  $a_1$  were varied simultaneously in order to ensure that the wave height remained fixed. Changes of this sort modify the period and the steepness of the solution simultaneously. The values of the corresponding  $\delta$ ,  $\epsilon$  and  $\Lambda$  are included in Table 3.

#### Observations:

- If  $k$  is small enough, there is no instability. If  $k$  is large enough, there is instability. This establishes that waves with sufficiently small steepness/amplitude are stable and that waves with sufficiently large steepness/amplitude are unstable.

Case III			
$k$	$\delta$	$\epsilon$	$\Lambda$
0.5	0.2967	0.0771	0.0458
0.9	0.1196	0.1376	0.0329
0.99	0.0715	0.1509	0.0216
0.999	0.0518	0.1551	0.0161

Table 3: The values of  $k$ ,  $\delta$ ,  $\epsilon$  and  $\Lambda$  for the Case III numerical simulations.

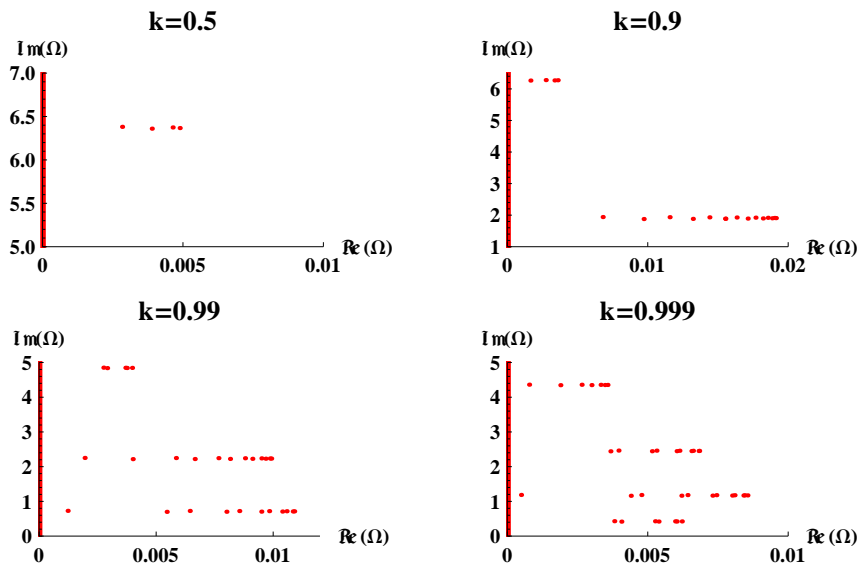


Figure 5: Results from Case III numerical simulations. A discrete representation of the spectra of (15) corresponding to  $a_1 k^2 = 0.1$ ,  $a_0 = 0.3$  and four different values of  $k$ .

- The cutoff between stability and instability occurs at  $k \approx 0.102$ .
- Each of the bands in the first quadrant is a compressed half oval. As  $k$  increases, the number of bands of instabilities increases.
- All instabilities are oscillatory.
- As  $k$  increases away from zero, the maximum growth rate increases until  $k \approx 0.86$ . Above this value, the maximum growth rate decreases. At  $k = 0.86$ , the maximum growth rate is 0.020.
- Generally, the instability with maximal growth rate is a  $\rho \neq 0$  perturbation.

Note that in all sets of simulations, as  $k \rightarrow 0$ ,  $\Re(\Omega) \rightarrow 0$ . This is consistent with the fact that  $k = 0$  corresponds to a stationary fluid with flat surface.

All of the instabilities presented herein have relatively small growth rates. These instabilities may not be physically observable due to dissipative or other physical effects because such effects may overwhelm any growth. Further, as  $k$  becomes very close to 1, the instability growth rate decreases (possibly to zero). This may explain the apparently stable Serre solitary waves created by Guizien & Barthélemy [10].

## 5 Summary

Several interesting properties of the system of nonlinear partial differential equations known as Serre equations were investigated in this article. We have shown that this system admits a closed-form three-parameter

family of periodic solutions that describe shallow-water wave propagation on horizontal bottoms. This is an important and desirable property that has not been previously demonstrated on a fully nonlinear set of Boussinesq-type equations. Moreover, the family of solutions limits to the Rayleigh solitary wave solution as  $k \rightarrow 1^-$  and to the trivial case of a fluid at rest when  $k \rightarrow 0^+$ .

We studied the linear stability of these solutions numerically through the Fourier-Floquet-Hill (FFH) method of Deconinck & Kutz [8]. Different combinations of parameter values were considered, while respecting their meaningful physical range. Spectral plots indicate that waves of small amplitude/steepness are stable while waves with sufficiently large amplitude/steepness are unstable. This result enforces some of the conclusions of Lannes & Bonneton [11] who demonstrate that Serre equations represent an appropriate model to describe nonlinear wave propagation in shallow water. Indeed, it appears that this weakly dispersive approximation of the full Euler system retains some degree of physical instability also contained in the Euler equations.

## Acknowledgments

This work was accomplished during a sabbatical leave of Professor John D. Carter at the Departamento de Ingeniería Hidráulica y Ambiental, Pontificia Universidad Católica de Chile (PUC). Financial support from the School of Engineering (PUC) and ECOS-Conicyt research grant No C07U01 are gratefully acknowledged.

## References

- [1] E. Barthélemy. Nonlinear shallow water theories for coastal waves. *Surveys in Geophysics*, 25:315–337, 2004.
- [2] J.L. Bona, M. Chen, and J.-C. Saut. Boussinesq equations and other systems for small-amplitude long waves in nonlinear dispersive media. I: Derivation and linear theory. *Journal of Nonlinear Science*, 12:283–318, 2002.
- [3] J. Boussinesq. Théorie des ondes et des remous qui se propagent le long d’un canal rectangulaire horizontal, en communiquant au liquide contenu dans ce canal des vitesses sensiblement pareilles de la surface au fond. *Journal de Mathématiques Pures et Appliquées*, 2:55–108, 1872.
- [4] P.F. Byrd and M.D. Friedman. *Handbook of Elliptic Integrals for Scientists and Engineers*. Springer-Verlag, New York, 1971.
- [5] R. Cienfuegos, E. Barthélemy, and P. Bonneton. A fourth-order compact finite volume scheme for fully nonlinear and weakly dispersive Boussinesq-type equations. Part I: Model development and analysis. *International Journal for Numerical Methods in Fluids*, 51:1217–1253, 2006.
- [6] R. Cienfuegos, E. Barthélemy, and P. Bonneton. A fourth-order compact finite volume scheme for fully nonlinear and weakly dispersive Boussinesq-type equations. Part II: Boundary conditions and validation. *International Journal for Numerical Methods in Fluids*, 53:1423–1455, 2007.
- [7] R. Cienfuegos, E. Barthélemy, and P. Bonneton. A wave-breaking model for Boussinesq-type equations including roller effects in the mass conservation equation. *Journal of Waterway, Port, Coastal, and Ocean Engineering*, 2009. In press.
- [8] B. Deconinck and J.N. Kutz. Computing spectra of linear operators using Hill’s method. *Journal of Computational Physics*, 219:296–321, 2006.
- [9] A.E. Green and P.M. Naghdi. A derivation of equations for wave propagation in water of variable depth. *Journal of Fluid Mechanics*, 78:237–246, 1976.
- [10] K. Guizien and E. Barthélemy. Accuracy of solitary wave generation by a piston wave maker. *Journal of Hydraulic Research*, 40(3):321–331, 2002.

- [11] D. Lannes and P. Bonneton. Derivation of asymptotic two-dimensional time-dependent equations for surface water wave propagation. *Physics of Fluids*, 21(1):016601, 2009.
- [12] P.A. Madsen and H.A. Schäffer. Higher-order Boussinesq-type equations for surface gravity waves: Derivation and analysis. *Philosophical Transactions of the Royal Society of London, Series A*, 356:3123–3184, 1998.
- [13] L. Rayleigh. On waves. *Philosophical Magazine*, 1(4):257–279, 1876.
- [14] F.J. Seabra-Santos, D.P. Renouard, and A.M. Temperville. Numerical and experimental study of the transformation of a solitary wave over a shelf or isolated obstacle. *Journal of Fluid Mechanics*, 176:117–134, 1987.
- [15] F. Serre. Contribution à l'étude des écoulements permanents et variables dans les canaux. *Houille Blanche*, 8:374–388, 1953.
- [16] F. Serre. Contribution à l'étude des écoulements permanents et variables dans les canaux. *Houille Blanche*, 8:830–872, 1953.
- [17] C.H. Su and C.S. Gardner. KDV equation and generalizations. Part III. Derivation of Korteweg-deVries equation and Burgers equation. *Journal of Mathematical Physics*, 10(3):536–539, 1969.